fuer Datumsformat

Weierstraß-Institut
für Angewandte Analysis und Stochastik

im Forschungsverbund Berlin e.V.

Stochastic Lagrangian footprint calculations over a surface with an abrupt change of roughness height

Orazgeldi Kurbanmuradov[1], Ullar Rannik[2], Alexander Levykin[4],
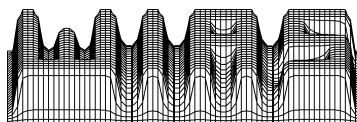
Karl K. Sabelfeld[3, 4], and Timo Vesala[2]

[1]	Center for Phys. Math. Research	[2]	Department of Physics,
	Turkmenian State University		FIN-00014 University of Helsinki,
	Turkmenbashy av. 31		Finland
	744000 Ashgabad, Turkmenistan		
[3]	Weierstrass Institute for Applied	[4]	Institute of Comput. Mathematics
	Analysis and Stochastics		and Mathematical Geophysics
	Mohrenstraße 39		Russian Academy of Sciences
	D – 10117 Berlin, Germany		Lavrentieva str., 6
	E-mail: sabelfel@wias-berlin.de		630090 Novosibirsk, Russia

No. 829

Berlin 2003

Abstract

Forward and backward stochastic Lagrangian trajectory simulation methods are developed to calculate the footprint and cumulative footprint functions of concentration and fluxes in the case when the ground surface has an abrupt change of the roughness height. The statistical characteristics to the stochastic model are extracted numerically from a closure model we developed for the atmospheric boundary layer. The flux footprint function is perturbed in comparison with the footprint function for surface without change in properties. The perturbation depends on the observation level as well as roughness change and distance from the observation point. It is concluded that the footprint function for horizontally homogeneous surface, widely used in estimation of sufficient fetch for measurements, can be seriously biased in many cases of practical importance.

1 Introduction

Over a horizontally homogeneous surface the flux measuered by micrometeorological technique equals to the surface flux. This principle is used to determine the surface exchange by the eddy covariance (EC) technique. The flux footprint function (e.g. Schmid, 1994) links the surface emissions to the observed fluxes above surface at EC measurement level. The footprint function is therefore used to estimate a distance required to make reliable EC meaurements, i.e. if the horizontal extent of underlying surface of interest is sufficient to determine its exchange rate. Extended tower measurements of fluxes over forests have been used during the last ten years to obtain detailed information on carbon and water exchanges between forest canopies and atmosphere. (Kaiser, 1998; Running, 1998; Valentini et al., 2000). Large areas of forest are not however common in Europe nor in the US. The footprint models based on analytical diffusion theory (Schuepp et al., 1990; Horst and Weil, 1992, 1994; Schmid, 1994) as well as Lagrangian stochastic simulation of ensemble of fluid parcel trajectories (Leclerc and Thurtell, 1990; Flesch, 1996; Baldocchi, 1997) assume horizontally homogeneous surface. For forest canopies the footprint models involve a number of uncertainties originating from the parametrization of the canopy turbulence features (Rannik et al., 2003). Such models are frequently applied to estimate the contribution of an area of certain upwind distance, or to estimate the fetch to ensure that the given area contributes a certain percent to observed flux, by vaguely assuming that the footprint function for horizontally homogeneous surface is a good approximation for more complex situation with changes in surface properties. In reality changes in surface roughness can be very drastic, for example in case of forest and field interface. Also the thermal inhomogeneities induced by albedo and repartioning of available energy into sensible and latent heat fluxes can be significant, this will be analised however in the second part of this paper. So we deal here with pure mechanical turbulence caused by the surface roughness.

One additional remark here should be made. Over rough surfaces, such as tall vegetation, vertical displacement of surface layer profiles occurs relative to ground surface. Displace-

ment height is usually 2/3 to 3/4 of the height of roughness elements, whereas the roughness length is usually 1/30 to 1/10 of the vegetation height. In this study the flow inside vegetation is not considered and the observation level (detector height) is equivalent to that of relative to diplacement height in real measurement setup. Displacement height would effectvely elevate flow streamlines and not affect the results qualitatively, whereas roughness change induces transition in horizontal wind speed and via mass conservation also non-zero vertical winds.

Lagrangian trajectory simulation can be used in the inhomogeneous flow field (e.g., see Thomson, 1987, and Kurbanmuradov, Sabelfeld, 2000). However, to make the stochastic trajectory simulation possible, the mean flow and some other statistical moments have to be found. We will extract this data from a closure model, conventionally obtained from the Reynolds-avergaing equations. The footprint function for inhomogeneous surface is estimated by backward Lagrangian trajectory simulation and the perturbations relative to footprint function for horizontally homogeneous case are analysed.

2   The governing equations

There exists a variety of closure models for turbulent mixing, ranging from constant eddy coefficient parametrization to detailed Large Eddy Simulations and Direct Numerical Simulation. As mentioned in [1], the performance of a k-model is almost identiacal to that of $k - \varepsilon$-model. We assume that the mean profiles in the boundary layer of atmosphere are described by the following system (Wager et.al., 1979):

$$
\begin{aligned}
u\frac{\partial u}{\partial x} + w\frac{\partial u}{\partial z} &= \frac{\partial}{\partial z}\, k\frac{\partial u}{\partial z} + f(v - G\sin\alpha), \\[2mm]
u\frac{\partial v}{\partial x} + w\frac{\partial v}{\partial z} &= \frac{\partial}{\partial z}\, k\frac{\partial v}{\partial z} - f(u - G\cos\alpha)
\end{aligned}
\tag{1}
$$

is the momentum equation, where the Cariolis parameter is given by $f = 2\Omega\sin\varphi$, $\Omega = 7.29\ 10^{-5}s^{-1}$, G is the geostrophical wind, and φ is the angle between the x-axis and the isobare; α is the angle between the x-axis and the direction of the geostrophical wind. Furhther,

$$
\frac{\partial u}{\partial x} + \frac{\partial w}{\partial z} = 0
$$

is the continuity equation, where k, is the turbulent exchange coefficient for the momentum. The balance of the kinetic energy is written as

$$
u\frac{\partial b}{\partial x} + w\frac{\partial b}{\partial z} = \alpha_b\frac{\partial}{\partial z}\, k\frac{\partial b}{\partial z} + k\left[\left(\frac{\partial u}{\partial z}\right)^2 + \left(\frac{\partial v}{\partial z}\right)^2\right] - \bar\varepsilon,
\tag{2}
$$

where $\bar\varepsilon = \frac{cb^2}{k}$ is the mean rate of dissipation of the turbulent energy, $c = 0.0286$, $\alpha_b \approx 0.7$. The functions k and b are related through

$$
l = \left(\frac{1}{\kappa z} + \frac{1}{l_0}\right)^{-1}, \quad k = C_k l\sqrt{b},
\tag{3}
$$

with $\kappa \approx 0.4$, $l_0 = 100$ m, $C_k = 0.41$. We deal in this first part of the paper with purely mechanical turbulence, and our system of governing equations consists of (1), (2) and the relation (3).

The functions vary in the layer $z_0 \leq z \leq h$, h being the height of the boundary layer, and z_0 the roughness height. The system of equations is considered with the following boundary conditions:

$$u = 0, \ v = 0, w = 0, \quad \text{at } z = z_0,$$
$$u = G \cos \alpha, \ v = G \sin \alpha \quad \text{at } z = h, \ x \leq 0,$$
$$\frac{\partial u}{\partial z} = \frac{\partial v}{\partial z} = 0 \text{ at } z = h, \ x > 0 \ ,$$
$$\frac{\partial b}{\partial z} = 0 \text{ at } z = z_0, \quad \text{an} d \ b = 0 \text{ at } z = h \ ,$$

At $z = z_0$ we take $l = \kappa z_0$.

2.1   Evaluation of footprint functions

We assume that our 3D flow is homogeneous in y-direction, and inhomogeneous in z- and x-directions. Roughness inhomogeneity along the x-direction only is assumed in our numerical analysis.

The flow is considered in the boundary layer of height h, with a roughness height $z_0 = z_{01}$ which is a constant for $x < 0$, then in a small interval $0 < x < \Delta$ it linearly changes from z_{01} to z_{02}, and then it is again constant: for $x > \Delta$ it equals to z_{02}. The detector is placed at a point (x_d, y_d, z_d). We will deal with the footprint function of concentration $c(x) = c(x; x_d, y_d, z_d)$ defined as the mean concentrtaion at the detector point from a linear source with the coordinate x, placed at roughness height, directed along the axis Y. Analogously is defined the footprint function of the vertical flux $q(x) = q(x; x_d, y_d, z_d) = \langle w(x_d, y_d, z_d) \, c'(x; x_d, y_d, z_d) \rangle$, where c' is the fluctuating part of the concentration.

The cumulative footprint functions of concentration and of vertical flux are defined as

$$C(x) = \int_x^\infty c(x')dx' \ , \quad Q(x) = \int_x^\infty q(x')dx' \ .$$

The normalized footprint function of flux is defined as $Q_n(x) = Q(x)/Q(-\infty)$. In this section we present the cumulative footprint functions for smooth-to-rough and rough-to-smooth changes of the roughness height.

We calculate the mean concentration c_i and q_{ix}, the vertical concentrtaion fluxes at the detector point, from a surface source uniformly distributed over strips of width $\Delta_i = b_i - a_i$: $D_i = \{ x, z : a_i \leq x \leq b_i \ z = z_0, \}$, $i = 1, \ldots, n_{sr}$. The corresponding cumulative and normalized cumulative footprint functions of flux are also calculated. Calculations are carried out for small values of Δ_i, and the result is then normalised by the strip width.

The forward simulation technique cannot be applied for estimation of concentration and flux exactly at a point in space in case of horizontally inhomogeneous turbulence, and/or exactly at moment t in case of non-stationary turbulence. Instead, one might consider averages over space and/or time localised near $\mathbf{x}$ and/or t (e.g., see Kurbanmuradov et al.,

3

1999). However, such a simulation might be computationally inefficient if the extention of the source is much larger than that of the detector. For these cases, the backward trajectory simulation, starting from the space-time point of interest, is more efficient (in the case of Eulerian approach see Sabelfeld, 1991, and in the Lagrangian framework see, e.g., Flesch and Wilson, 1995).

To be more specific, let us present now the backward estimators for the evaluation of footprint functions in the case of the boundary layer with the sources uniformly distributed over the strips D_i, $i = 1, \ldots, n_{sr}$. For simplicity, we have taken the x-axis coincident with the direction of the geostrophical wind, i.e., $\alpha = 0$.

The backward trajectory starts at time t, at the detector point with the velocity sampled from the Eulerian velocity pdf $p_E(u, x)$ which is assumed to be Gaussian, see Appendix II. We note only that below, we denote by $\bar{u}_{Ek}$ the k-th component ($k = 1, 2, 3$) of the mean Eulerian velocity vector, and the hat over the symbols x and u is to indicate that this is a finite-diffrence approximation to the true Lagrangian trajectory.

The backward trajectory simulation is conveniently carried out through the semi-implicit Euler scheme, which can be written for one time step as follows:

$$\hat{x}_k(t - \Delta t) = \hat{x}_k(t) - (\hat{u}'_k(t) + \bar{u}_{Ek}(t, \hat{x}(t))) \, \Delta t,$$

$$\hat{u}'_k(t - \Delta t) = \hat{u}'_k(t) - \hat{a}'_k(t, \hat{x}(t - \Delta t), \hat{u}(t)) \, \Delta t + \sqrt{C_0 \bar{\varepsilon}(t - \Delta t, \hat{x}(t - \Delta t)) \, \Delta t} \, \eta_{tk},$$

where η_{tk}, $k = 1, 2, 3$ are independent standard gaussian random variables. Here for a reason of practical convenience, we work in the "primed" velocity variables $\hat{u}'_k = \hat{u}_k - \bar{u}_{Ek}$, so that

$$\begin{aligned} d\hat{x}_k &= (\hat{u}'_k + \bar{u}_{Ek}) \, ds \, , \\ d\hat{u}'_k &= \hat{a}'_k \, ds + \sqrt{C_0 \bar{\varepsilon}} \, \overleftarrow{d} \, W_k(s), \quad s < t, \; k = 1, 2, 3, \end{aligned}$$

with the condition that the trajectory starts at the detector position with the velocity sampled from the Gaussian pdf p_E. Here according the formula given in Appendix II we have

$$\begin{aligned} \hat{a}'_k &= \hat{a}_k - \frac{\partial \bar{u}_{Ek}}{\partial x_j} \bar{u}_{Ej} - \frac{\partial \bar{u}_{Ek}}{\partial x_j} \hat{u}'_j \\ &= \frac{C_0 \bar{\varepsilon}}{2} \lambda_{kj} \hat{u}'_j + \frac{1}{2} \frac{\partial \sigma_{kj}}{\partial x_j} + \frac{\lambda_{km}}{2} \bar{u}_{Ei} \frac{\partial \sigma_{jm}}{\partial x_i} \hat{u}'_j + \frac{\lambda_{km}}{2} \frac{\partial \sigma_{im}}{\partial x_j} \hat{u}'_j \hat{u}'_i \\ &= \hat{\alpha}_k + \hat{\beta}_{kj} \, \hat{u}'_j + \gamma_{kji} \, \hat{u}'_j \hat{u}'_i \, , \end{aligned}$$

and

$$\hat{\alpha}_k = \frac{1}{2} \frac{\partial \sigma_{kj}}{\partial x_j} \, , \quad \hat{\beta}_{kj} = \frac{C_0 \bar{\varepsilon}}{2} \lambda_{kj} + \frac{\lambda_{km}}{2} \bar{u}_{Ei} \frac{\partial \sigma_{jm}}{\partial x_i} \, , \quad \gamma_{kji} = \frac{\lambda_{km}}{2} \frac{\partial \sigma_{im}}{\partial x_j} \, .$$

All the expressions for the input functions are given in Appendices.

Recall that we use here the summation convention taking the sum over repeated indeces $i, j, l = 1, 2, 3$, and $\overleftarrow{d} \, W_k(s)$ stands for the backward Wiener differential (see Kurbanmuradov, Sabelfeld, 2000) which implies for the Euler scheme that the increments are taken back in time.

Let us denote by τ_{ij} the time at which the trajectory $(\hat{\mathbf{x}}(s), \hat{\mathbf{u}}(s))$, $s \leq t$ reaches the ground surface and touches the i-th strip: the first touchdown at τ_{i1}, the second (after a reflection from the boundary) at τ_{i2}. etc., and the last one at τ_{iN_i}. The random estimators have the following form (see Appendix II), for the concentration,

$$c_i = \left\langle \sum_{j=1}^{N_i} \frac{2}{\Delta_i} \frac{1}{|\hat{u}_3(\tau_{ij})|} \right\rangle \, ,$$

and for the vertical flux:

$$q_{iz} = \left\langle \sum_{j=1}^{N_i} \frac{2}{\Delta_i} \frac{\hat{u}_3(t)}{|\hat{u}_3(\tau_{ij})|} \right\rangle \, , \quad i = 1, \ldots, n_{sr}.$$

Here the angle brackets stands for the averaging over the ensemble of independent backward trajectories.

3 Results

We study in this section the impact of the roughness change on the footprint functions. The developed code calculates the footprint and cumulative footprint functions of concentration and flux for the horizontally inhomogeneous case when the roughness height is constant z_{01} for $x < 0$, then in a small interval $0 < x < \Delta$ it linearly changes from z_{01} to z_{02}, and then it is again constant: for $x > \Delta$ it equals to z_{02}. In calculations, we have taken $\Delta = |z_{02} - z_{01}|$. Note that when we speak about the inhomogeneous case, two essentially different cases are considered: $z_{01} < z_{02}$ (smooth-to-rough) and $z_{01} > z_{02}$ (rough-to-smooth).

To be specific, we have taken in all calculations the geostrophical wind as $G = 10\text{m/s}$, and the boundary layer height as $h = 1\text{km}$. So the spatial scale in the figures is given in km. To give a sensitivity analysis to the change of these parameters, we present simultaneously the footprint functions of the inhomogeneous and homogeneous cases with the corresponding roughness height. These enables us to find the regions of applicability of the results obtained for the homogeneous case and moreover, to conclude where the inhomogeneous case shows considerable differences compared to the homogeneous roughness. We present also some other footprints, in particular, the cumulative footprint functions of concentration and vertical flux. In all calculations we run $4\,10^5$ backward trajectories, the strip width was 2 m, the time step was varying according to $\Delta t = 0.025\tau$, where $\tau = 2\sigma_w^2/(C_0\bar{\varepsilon})$ is the Lagrangian time scale at the trajectory instantaneous position. Since the variance of the random estimators was large, we have made a gaussian smoothing procedure with a band width equal to 4 strip widths.

3.1 Footprint functions of concentrtaion and flux

Let us describe the results of numerical simulations. We have made the calculations for two different cases: (1) smooth-to-rough, and (2) rough-to-smooth change of the roughness height. The detector was placed at the height $z_d = 2$ m, at a distance x_d.

Smooth-to-rough case.

In these calculations, along with the inhomogeneous case, we plot simultaneously the footprint functions for the homogeneous case with roughness height $z_0 = z_{02}$.

In Figure 1, left picture, we present the footprint function of concentration for the case of roughness change indicated above, for $x_d = 20$ m, $x_d = 50$ m and $x_d = 100$ m (the same curve is given for the homogeneous case at $z_0 = 5$ cm) as functions of the dimensionless upwind distance X/h, where the upwind distance X is defined as $X = -x + x_d$ - the distance to the detector. The same curves are shown in the right picture for the case $z_{01} = 1$ cm, $z_{02} = 25$ cm.

It is seen that the footprint functions of concentration for inhomogeneous cases are all smaller compared to the homogeneous case in the near-region which is $X/h < 0.04$ in the left picture, and $X/h < 0.08$ in the right picture. In the far-region the situation is reverse: all the inhomogeneous curves are over the homogeneous curve after $X/h > 0.15$.

The inhomogeneous curves have local minima at the position of roughness change; after this point they increase and become higher than the homogeneous curve. It is clearly seen that the minima are more pronounced in the case of larger roughness change. Note that this behaviour explains why the homogeneous curve in the left picture of Figure 2 (presenting the corresponding cumulative footprint function of concentrtaion) is higher than all the curves for the small upwind distances, and then decreases down all the curves; here we give more detailed dependence on x_d starting from $x_d = 20$ m, with the last value $x_d = 200$ m, where the influence of the roughness change is expected to be almost disappeared. The same is true for the right picture (note that we have shown the curves only for distances $X/h < 1$, therefore we cannot see the position where the homogeneous curve is down all the inhomogeneous curves but in calculations it happened).

In Figure 3 we present the corresponding footprint functions of flux, for the case of small (left picture) and larger roughness change (right picture). Note that here the difference between the homogeneous and inhomogeneous curves in the near-region is in the case of larger roughness change (right picture) much higher than that of smaller roughness change (left picture). In all cases the homogeneous curve is positioned almost everywhere down the inhomogeneous curves; one exception is in the neighbourhood of the roughness change which is clearly seen in the right picture for the case $x_d = 20$ m.

In Figure 4 the cumulative footprint function of flux Q is presented. It is clearly seen that the difference between the homogeneous and inhomogeneous curves is becoming less and less as the value of x_d increases. Note that the homogeneous curve tends to 1 as the upwind distance increases while in the inhomogeneous case, the curves tend to asymptotic values which are larger than 1. To find the footprint area, it is convenient to use the normalized cumulative footprint function of flux which is defined as the cumulative footprint function of flux divided by the corresponding asymptotic value. These curves are shown in Figure 5. For illustration, here we show through a horizonatal dashed line the level of 90% contribution to the detector made by the surface around the detector position. Calculations show that the fetch in the homogeneous case is smaller than that of inhomogeneous case; from Fig.5 it seen that the corresponding fetch in the homogeneous case is about 200 m, while for $x_d = 20$ m it is about two times larger. From this picture we can conclude that the inhomogeneous case with $x_d = 200$ m is approximately coincident with the homogeneous case, hence the analytical formulae known for the homogeneous case can be applied inside

the region whose diameter is not less than 200 m. For $x_d < 200$ m, the change of roughness should be taken into account. This confirms the known practical recommendation saying that the inhomogeneity can be neglected if $x_d/z_d > 100$.

Rough-to-Smooth case.

We present here the calculations for the rough-to-smooth case showing the same footprint functions plotted in Figures 1-5. These footprint functions when compared to the corresponding footprint functions presented in Figures 1-5 have the following features: the local minima at the roughness change in Figs.1,3 correspond to the local maxima in Figs.6,8. Also, in Figs.6,8 the homogeneous curve is down the inhomogeneous curves, in the near-region, while in the far-region it is over these curves. The same is true for the cumulative footprint functions plotted in Figs.7,9. Note that in the inhomogeneous case, the asymptotic value of cumulative footprint functions of flux at large distances is less than 1; it is seen that the smaller x_d, the smaller this asymptotic value. For larger roughness change it is becoming even less.

As to the fetch, we can conclude from Fig.10 that in contrast to the smooth-to-rough case, here the fetch of homogeneous case is larger than that of the inhomogeneous cases; for instance, in the case of the roughness change $z_{01} = 25$ cm, $z_{02} = 1$ cm, the fetch is about 80 m for $x_d = 50$ m, while for the homogeneous case it is about 300 m.

Some features of the qualitative behaviour of the footprint functions

Let us describe some features of the qualitative behaviour of the footprint functions for the inhomogeneous case. In Figure 11 we plot the homogeneous curves for two cases of the roughness height: $z_0 = 1$ cm and $z_0 = 25$ cm, and the inhomogeneous curves for the case of roughness change from $z_{01} = 1$ cm to $z_{02} = 25$ cm (left picture: the footprint of concentrtaion, and the right picture: the footprint function of flux). The position of the roughness change is shown by the dashed vertical line.

First consider the results plotted in the left picture. In the near-region (left to the dashed vertical line) the inhomogeneous curve behaves qualitatively as the homogeneous curve for $z_0 = 25$ cm, lying however considerably below with its maximum position shifted to the left (closer to the detector) when compared with the maximum position of the homogeneous curve. In the region $X/h > 0.08$ we observe a qualitatively similar behaviour of the inhomogeneous curve and the homogeneous curve but for $z_0 = 1$ cm; the curves are converging in the far-region. The maximum position of the inhomogeneous curve is shifted to the right. Thus the qualitative behaviour of the inhomogeneous curve is controlled by the two homogeneous curves, - in the close-region by the case $z_0 = 25$ cm, and in the far-region by the case $z_0 = 1$ cm. This leads to the bimodal shape of the inhomogeneous curve. But from a simple superposition of the two homogeneous footprint functions we could not expect such a deep drop between the two modes. This drop is caused by the flow structure around the change of roughness: in contrast to the homogeneous case here we have positive vertical component of the mean velocity. This implies that an additional part of the emitted particles miss the

Generally, the same arguments are true for the footprint function of flux shown in the right picture of Fig.11, with not so deep drop between the two modes. This can be explained by the fact that the maximum position of the homogeneous curve with $z_0 = 1$ cm is closer to the roughness jump.

Note that from this picture we can clearly seen that the cumulative footprint function of flux Q for the inhomogeneous case is larger than 1 in contrast to the homogeneous case where it is always less than 1. Indeed notice that the area under the homogeneous curve $z_0 = 25$ cm equals 1, so if we take the area under the homogeneous curve $z_0 = 25$ cm in the region $X < x_d$ and add the area under the homogeneous curve $z_0 = 1$ cm in the region $X > x_d$ we get a value which is larger than 1 which follows from a simple comparison of the curves behaviour.

Let us turn to the rough-to-smooth case. In Figure 12 we plot the same curves as in Figure 11, but for the roughness change from $z_{01} = 25$ cm to $z_{01} = 1$ cm. At the roughness change position we observe a small jump in the inhomogeneous curve presenting the footprint function of concentrtaion (left picture). Again, the general form of this curve can be deduced from the superposition of the two homogeneous curves, while the jump can be explained here by the negative values of the vertical component of the mean flow around the roughness change.

An analysis of the footprint function of flux (right picture) analogous to that made for the smooth-to-rough case above shows that the cumulative footprint function of flux can here be less than 1.

A larger change of the roughness height

Further we have made calculations for the larger change of the roughness height, namely, for $z_{01} = 1$ cm, $z_{02} = 100$ cm in the smooth-to-rough case, and $z_{01} = 100$ cm, $z_{02} = 1$ cm in the rough-to-smooth case. The detector height was taken at $z_d = 20$ m. The relevant footprint functions of concentration are shown in Figure 13, the footprint functions of flux q - in Figure 14, and the cumulative footprint functions of flux Q - in Figure 15, for different values of x_d. The results are in a good agreement with the conclusions made for the smaller change of the roughness height, showing even more clear the qualitative behaviour of the curves discussed above. It should be noted that in this case we cannot expect a good quantitative prediction because for the high roughness height we need to make a correction of the mean flow model which takes into account that the inhomogeneity affects the mean flow in a more complicated manner.

Dependence on the detector height z_d.

Let us now consider the dependence of the footprint functions on the detector height z_d. In Figure 16 we present the footprint functions of concentration (left picture, in log-log scale) and flux (right picture, in log-line scale) for the smooth-to-rough case ($z_{01} = 1$ cm, $z_{01} = 25$ cm; the x -coordinate of the detector is fixed at $x_d = 100$ m, and its height is varying from $z_d = 2$ m to $z_d = 16$ m. In the left picture it is seen that the local minima can be observed in all curves, but the higher the detector, the smaller the drop whose width is becoming larger with the height. The influence of the roughness change on the footprint function of flux is observable (right picture) till the height of about $z_d = 16$ m.

The corresponding cumulative footprint functions of concetration C (left picture) and flux Q (right picture) are shown in Figure 17. Note that the function C is uniformly decreased (in the considered region) with the height z_d. For the function Q this is not the case: the curve for $z_d = 4$ m is first rapidly increasing being larger than all the other curves, and then is slowing down and finally tends to its asymptotic value at distances (about $X/h \sim 1$) where the other curves are still increasing. Note that there is no monotonic

beahviour of the asymptotics $Q(X/h)$ at large values of X/h: first it increases with height - z_d for $z_d = 4$ m it is smaller than that for $z_d = 8$ while for $z_d = 32$ m the value is the smallest compared to all other values. This can be explained as follows. When the height z_d is small, the detector is well inside the inner boundary layer generated by the roughness change, and the situation is close to the homogeneous case (with the roughness height $z_0 = z_{02}$) where the asymptotic value is 1. For large heights z_d (larger than the height of the inner boundary layer) we are again in the situation close to the homogeneous case with the roughness height $z_0 = z_{01}$, therefore the corresponding asymptotics is again close to 1. In between, for intermediate heights, the asymptotic value is larger than 1 (e.g., for $z_d = 4, 8, 16$ m). The additional contribution is coming from the trajectories with positive vertical velocities in the neighbourood of the position of the roughness change (the source is in a sense effectively lifted). The same arguments are true for the rough-to-smooth case with the feature that in the intermediate heights the asymptotic values are less than 1 because in this case the trajectories get negative vertical velocities at the position of the roughness change. It should be noted that if we define the cumulative footprint function differently by omitting the convective part $< w >< c >$, i.e., as $Q_t = < w' c' >$, then the above mentioned asymptotics is almost always true for Q_t. This holds for the smooth-to-rough case while for the rough-to-smooth case it is true only for large values of x_d ($x_d > 20 z_d$), see Figure 18.

4   Discussion and conclusions

A closure model is used to evaluate the mean flow and the Reynolds stress tensor required in the stochastic Lagrangian model we applied to calculate the footprint functions of concentration and its horizontal and vertical fluxes. This model provides the mean velocities and other characteristics of the flow over the roughness height.

A sensitivity analysis is made for the footprint functions under perturbation of the roughness height; two cases are considered: (1) smooth-to-rough, and (2) rough-to-smooth change of the roughness height. The calculations show that the footprint function of concentration is more sensitive than that of the vertical flux.

It is concluded that the footprint and cumulative footprint functions of concentration for horizontally homogeneous surface, widely used in estimation of sufficient fetch for measurements, can be seriously biased in many cases of practical importance. The calculations show that the footprint area based on the cumulative concentrations if estimated through the homogeneous case can be essentially under- or overestimated, compared to the true inhomogeneous case. For instance, in the case when the detector is placed at $x_d = 100$ m from the roughness jump (from $z_{01} = 1$ cm to $z_{02} = 25$ cm), at the height $z_d = 2$ m, the fetch calculated from the homogeneous curve is about 100 m, while the inhomogeneous curve predicts the fetch of 400 m (see the right picture of Fig.5). In the smooth-to-rough case, the cumulative footprint function of flux for the inhomogeneous case is larger than 1 in contrast to the homogeneous case where it is always less than 1. In the rough-to-smooth case the situation is different: the cumulative footprint function of flux can here be considerably less than 1. However the 1-normalization is true if only the turbulent contribution to this flux is evaluated, i.e., omitting the "advecting part" $< w >< c >$. This holds for the smoot-to-rough case while for the rough-to-smooth case it is true only for large values of x_d ($x_d > 20 z_d$).
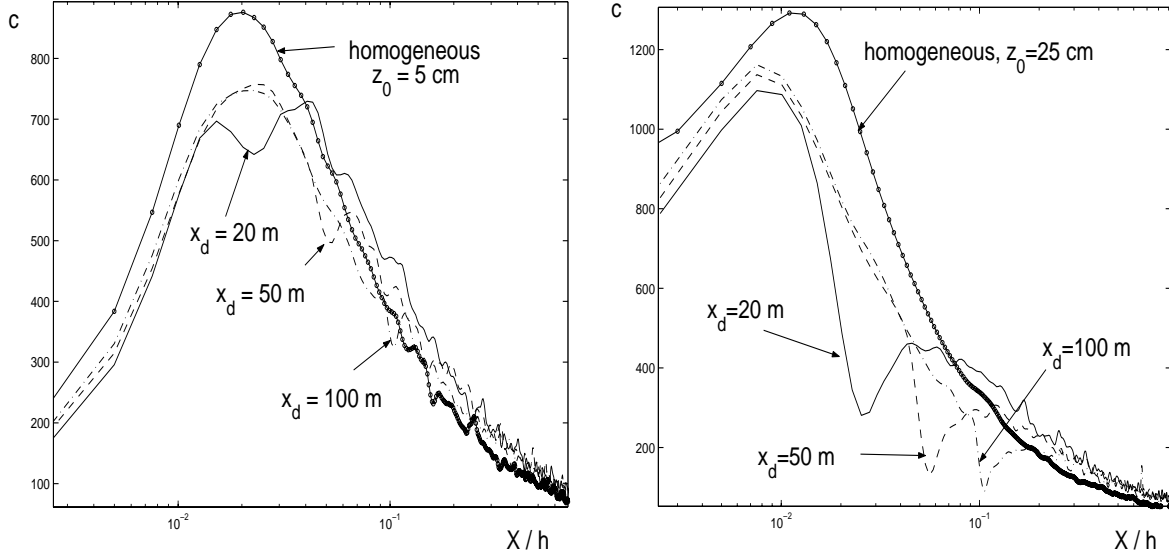
Figure 1: The footprint function of concentration c ($z_{01} = 1$ cm, $z_{02} = 5$ cm, left picture, and $z_{01} = 1$ cm, $z_{02} = 25$ cm, right picture), versus the dimensionless upwind distance X/h, for different values of x_d.
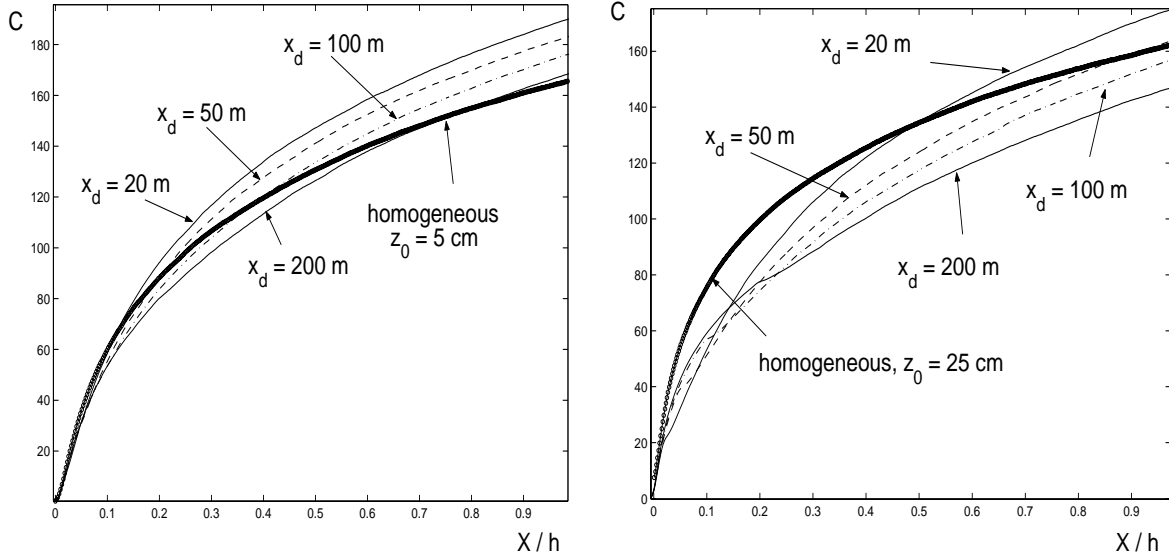

Figure 2: The cumulative footprint functions of concentrtaion C, versus the dimensionless upwind distance X/h, for different values of x_d. The roughness change is the same as in Figure 1.
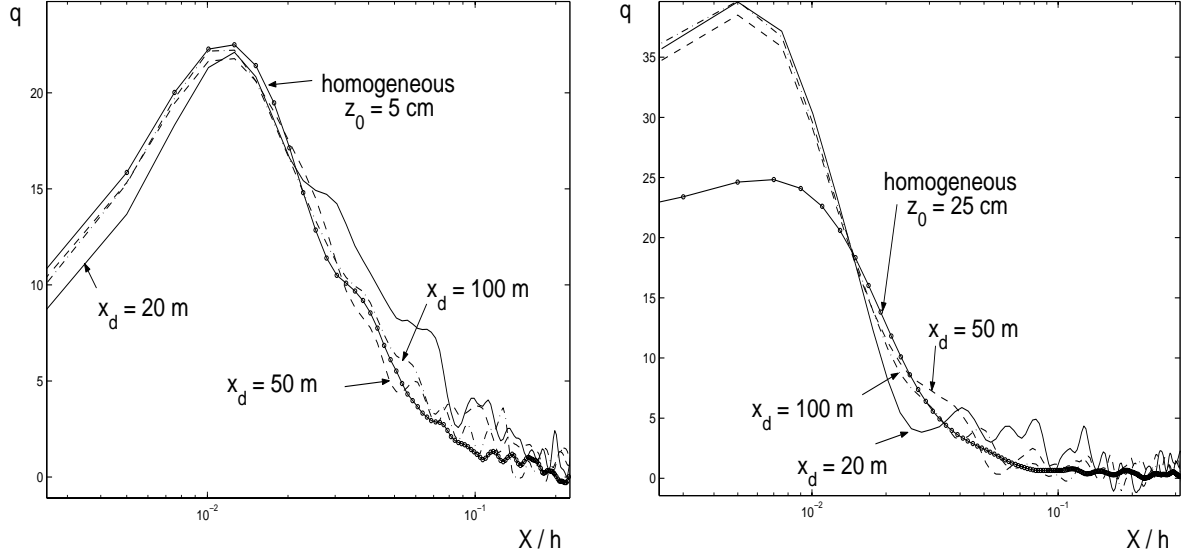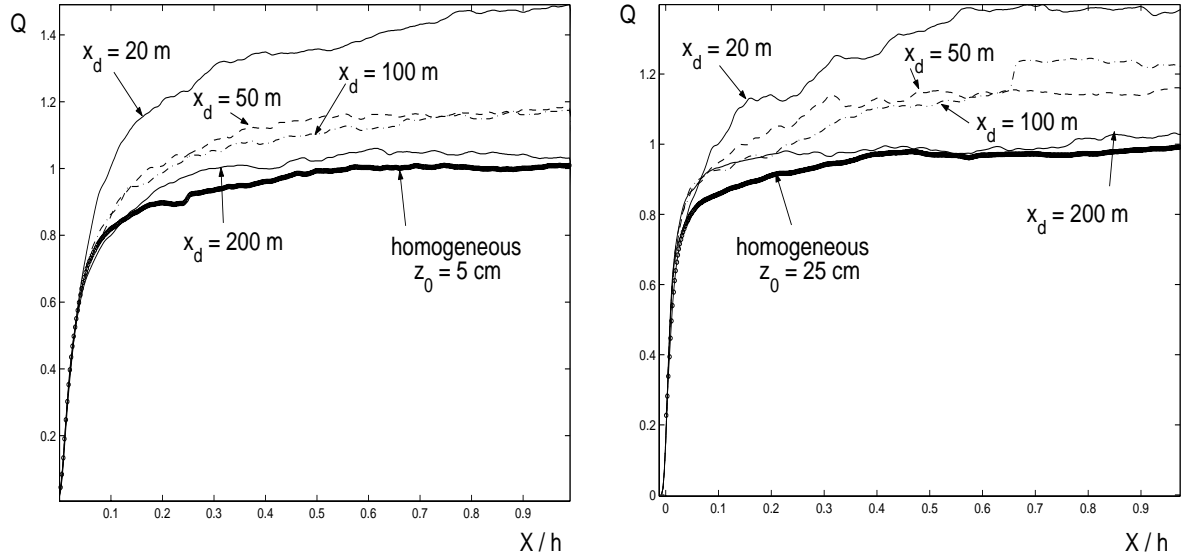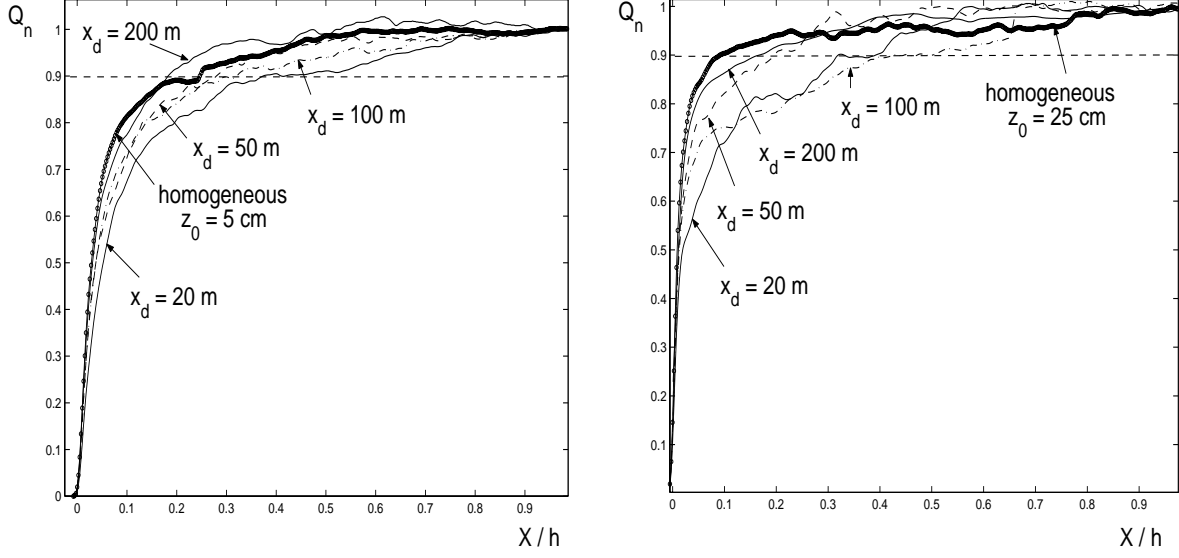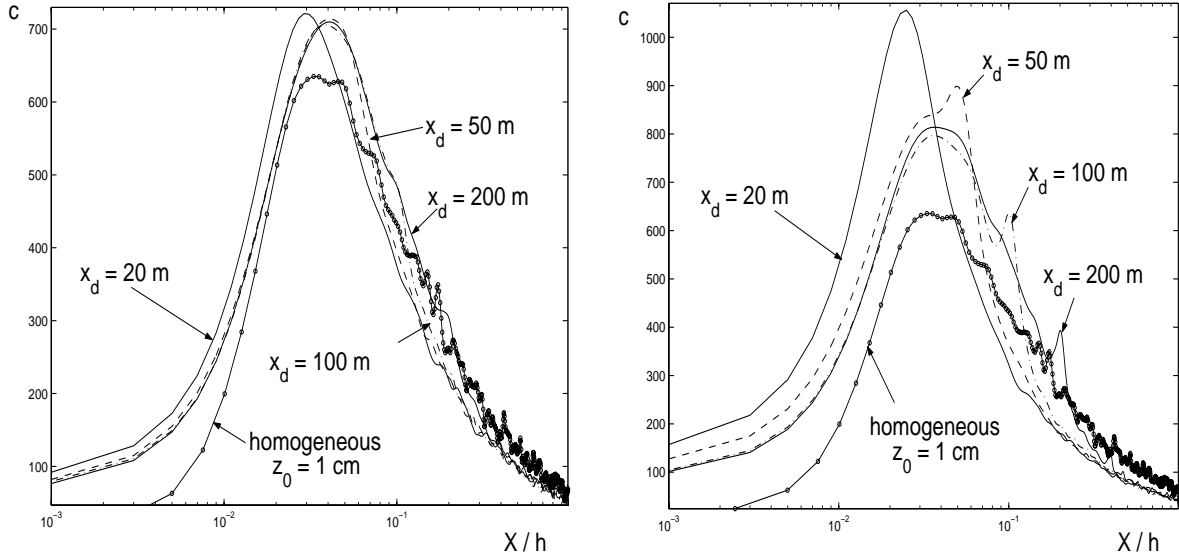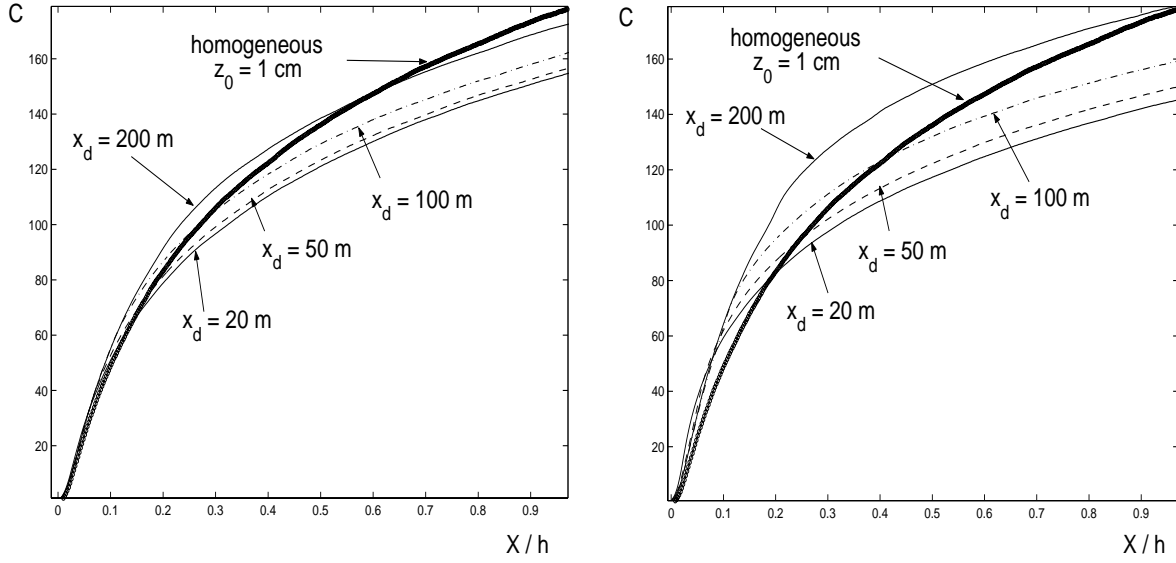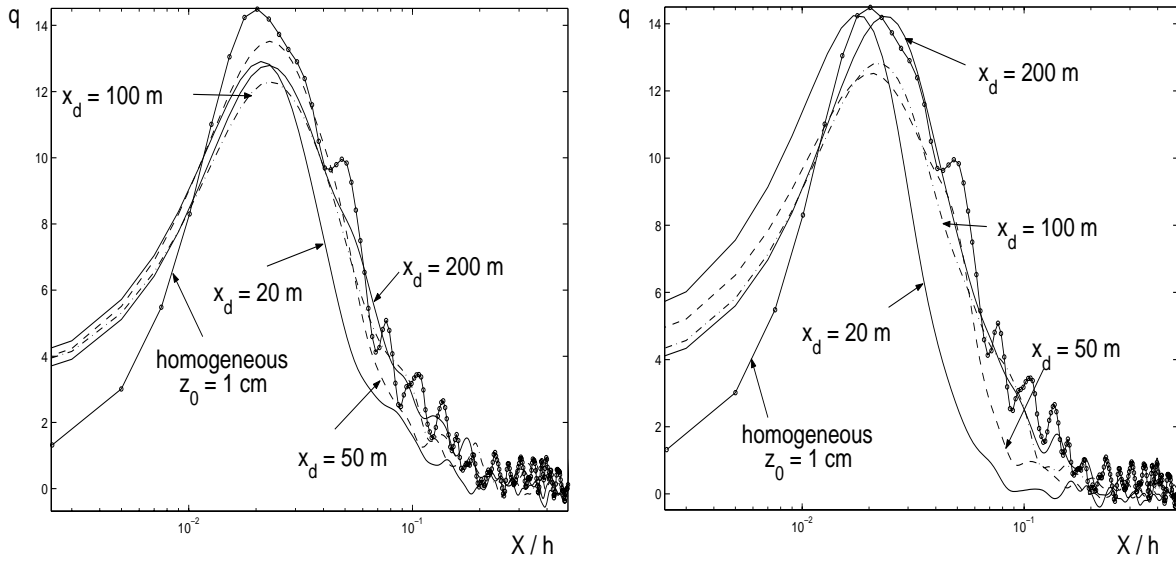
10

Figure 3: The footprint function of flux q ($z_{01} = 1$ cm, $z_{02} = 5$ cm, left picture, and $z_{01} = 1$ cm, $z_{02} = 25$ cm, right picture), versus the dimensionless upwind distance X/h, for different values of x_d.

Figure 4: The cumulative footprint functions of flux Q, versus the dimensionless upwind distance X/h, for different values of x_d. The roughness change is the same as in Figure 3.

Figure 5: The normalized cumulative footprint functions of flux Q, versus the dimensionless upwind distance X/h, for different values of x_d. The roughness change is the same as in Figure 3.

Figure 6: The footprint function of concentration c ($z_{01} = 5$ cm, $z_{02} = 1$ cm, left picture, and $z_{01} = 25$ cm, $z_{02} = 1$ cm, right picture), versus the dimensionless upwind distance X/h, for different values of x_d.

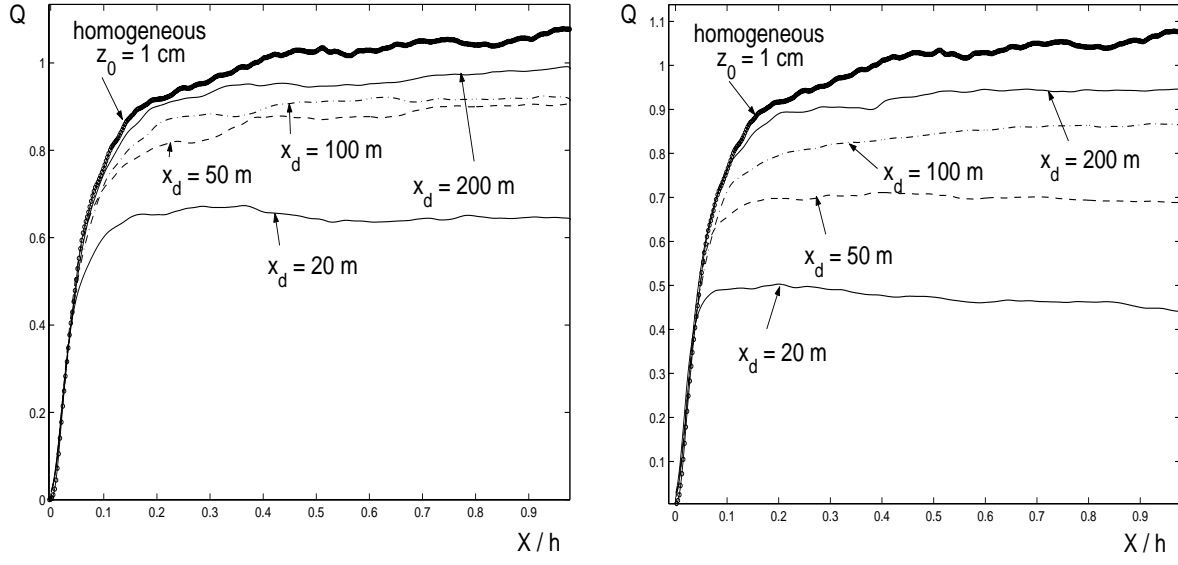Figure 7: The cumulative footprint functions of concentrtaion C, versus the dimensionless upwind distance X/h, for different values of x_d. The roughness change is the same as in Figure 6.

Figure 8: The footprint function of flux q ($z_{01} = 5$ cm, $z_{02} = 1$ cm, left picture, and $z_{01} = 25$ cm, $z_{02} = 1$ cm, right picture), versus the dimensionless upwind distance X/h, for different values of x_d.

Figure 9: The cumulative footprint functions of flux Q, versus the dimensionless upwind distance X/h, for different values of x_d. The roughness change is the same as in Figure 8.
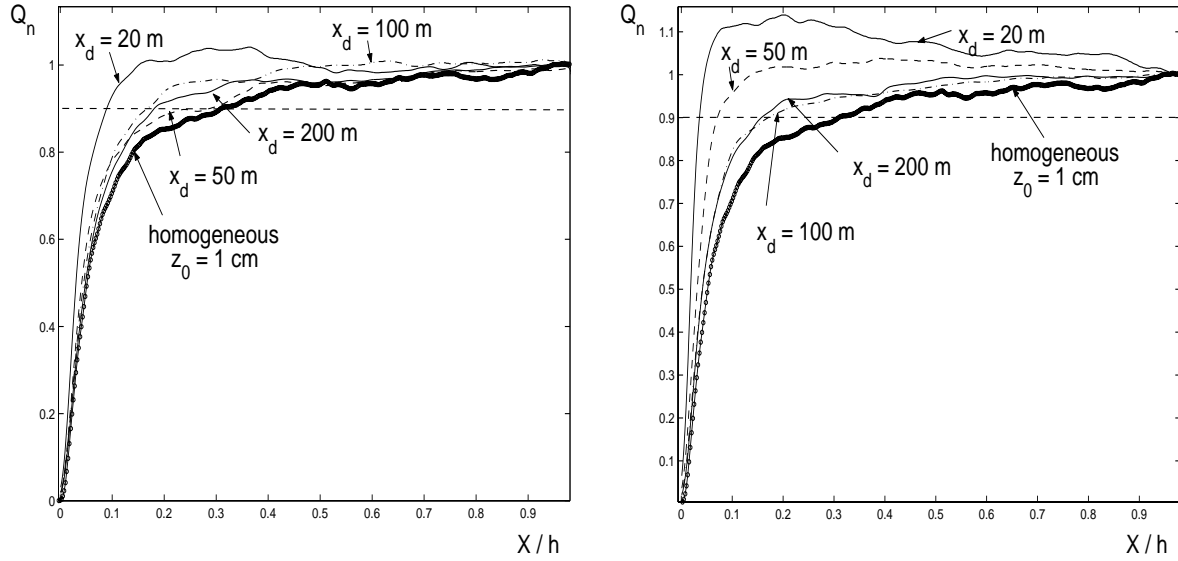

Figure 10: The normalized cumulative footprint functions of flux Q, versus the dimensionless upwind distance X/h, for different values of x_d. The roughness change is the same as in Figure 8.
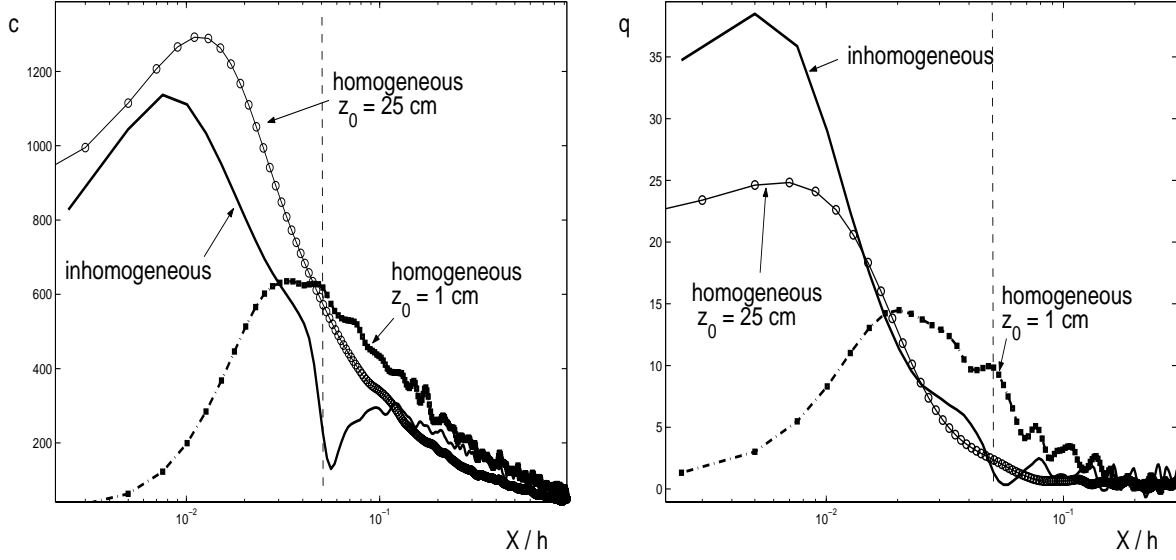
Figure 11: The footprint functions of concentration c (left picture) and flux q (right picture). For comparison, three curves are shown: the homogeneous curves for $z_0 = 1$ cm and $z_0 = 25$ cm, and the inhomogeneous curve for the roughness change from $z_0 = 1$ cm to $z_0 = 25$ cm, for $x_d = 50$ m.
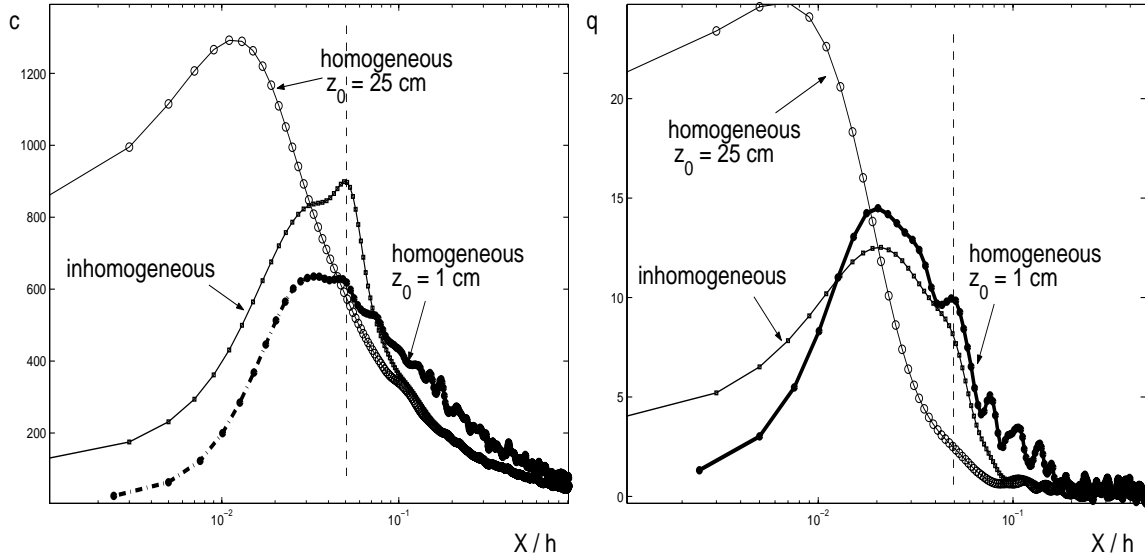

Figure 12: The same as in Figure 11, but for the rough-to-smooth case: the roughness change from $z_0 = 25$ cm to $z_0 = 1$ cm,
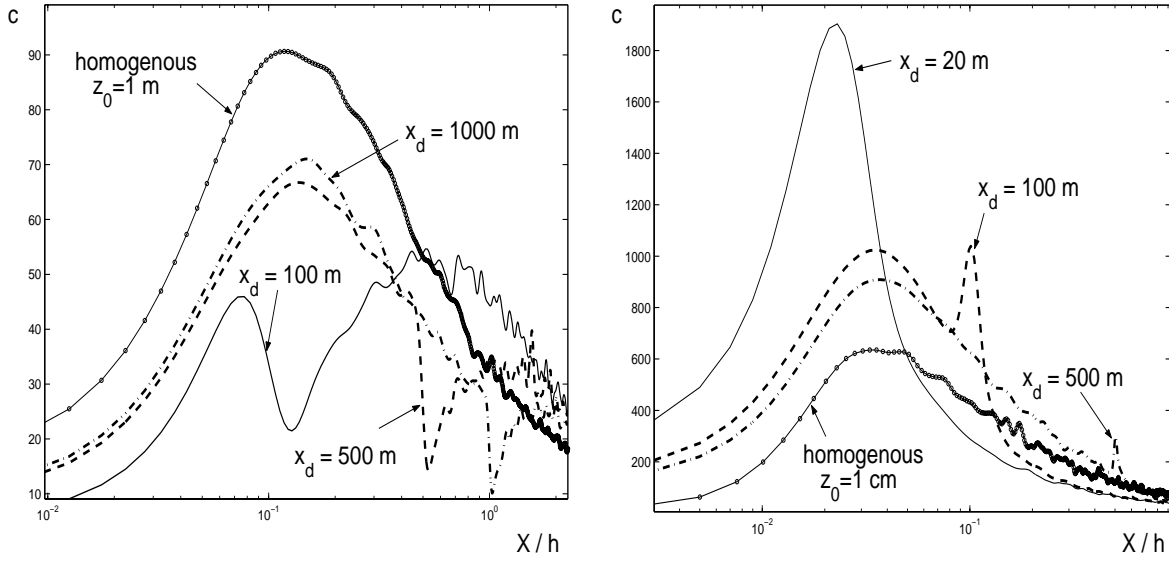
Figure 13: The footprint function of concentration for the smooth-to-rough case, the roughness height changes from $z_{01} = 1$ cm to $z_{02} = 100$ cm (left picture), and rough-to-smooth case with $z_{01} = 1$ cm, $z_{02} = 100$ cm (right picture). In all curves, $z_d = 20$ m.
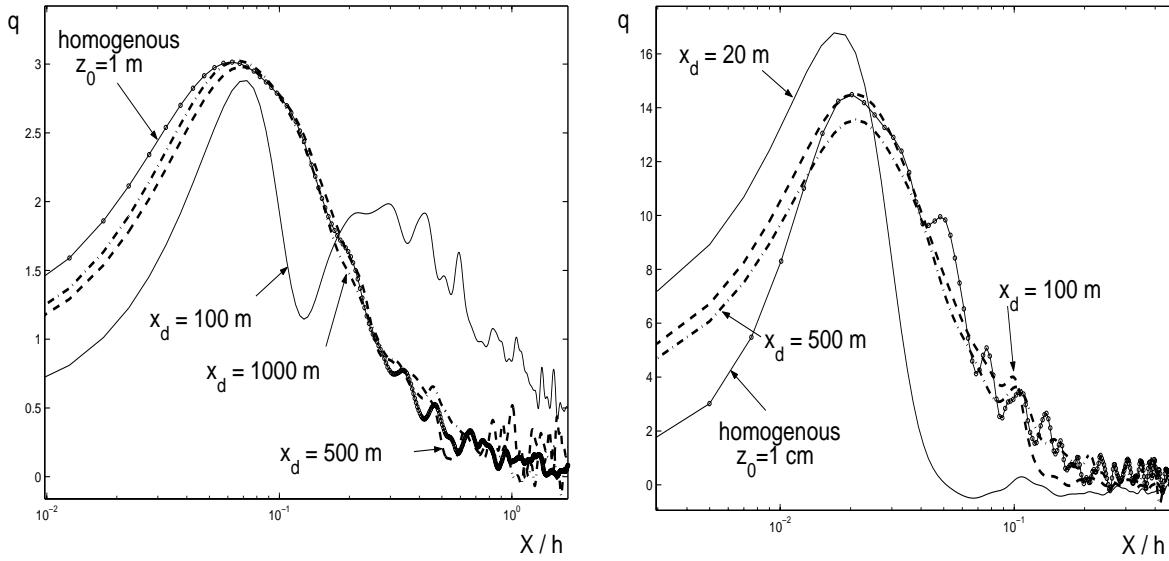
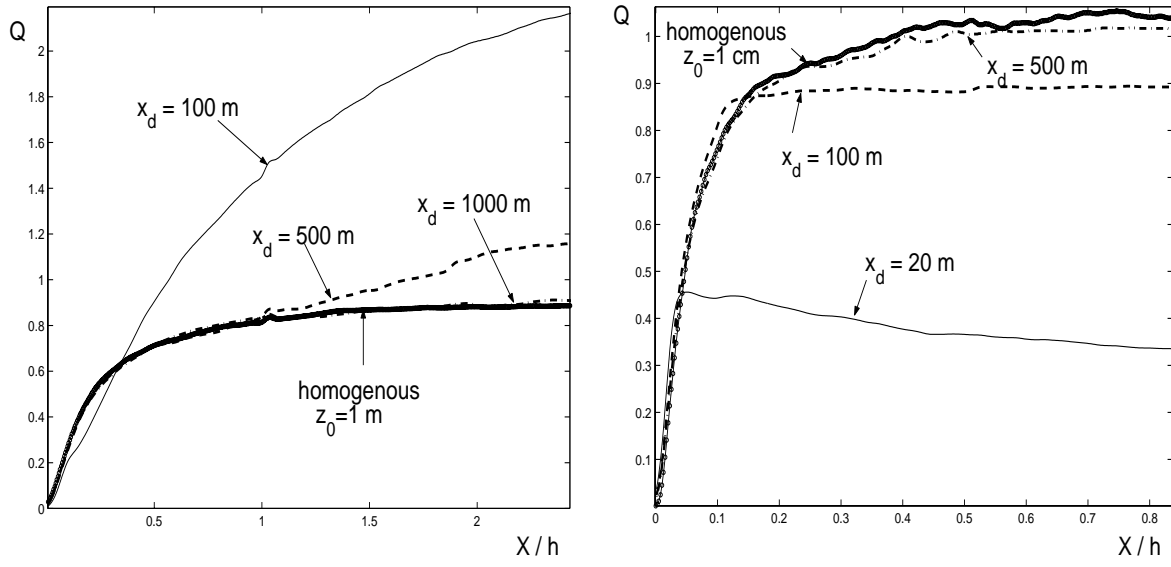Figure 14: The same as in Figure 13, but for the footprint function of flux q.

Figure 15: The same as in Figure 13, but for the cumulative footprint function of flux Q.
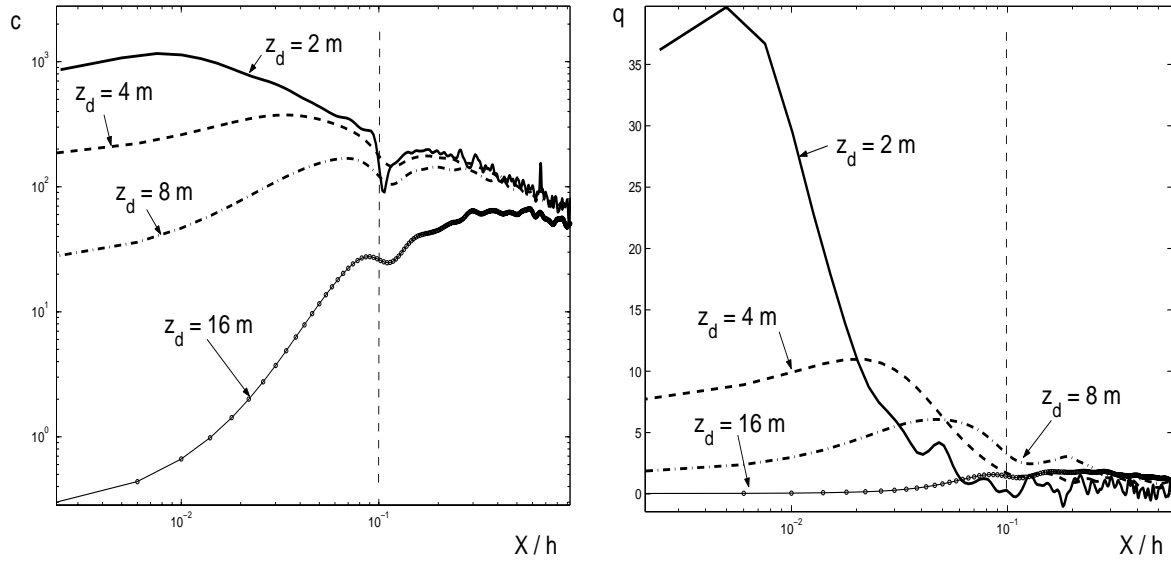

Figure 16: The footprint functions of concentration c (left picture) and flux q (right picture), for $x_d = 100$ m, and different values of the detector heights z_d.
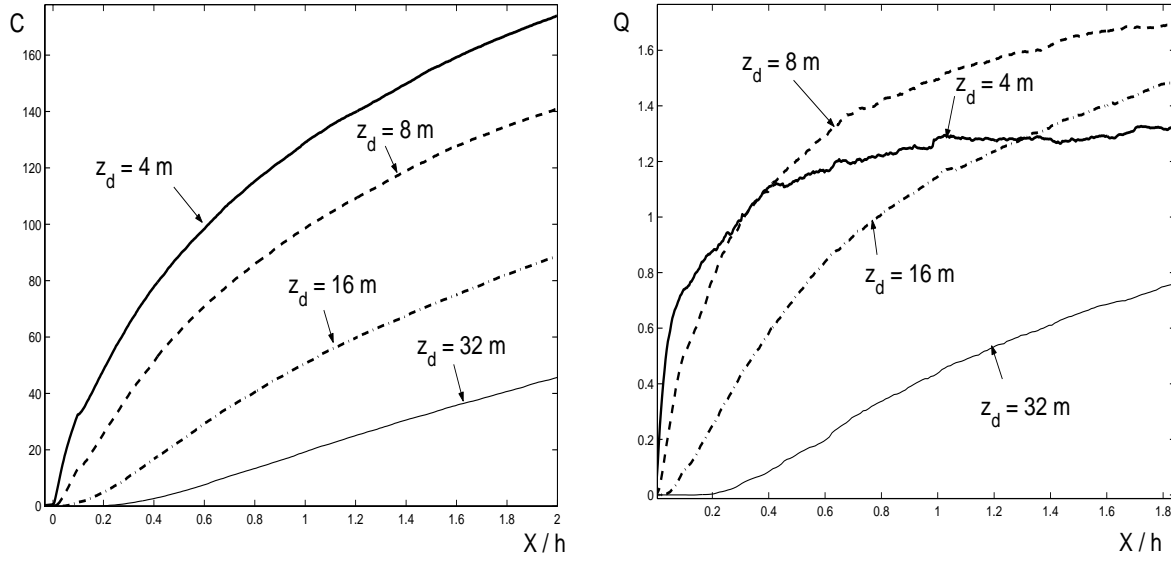
Figure 17: The cumulative footprint functions of concentration C (left picture) and flux Q (right picture), for $x_d = 100$ m, and different values of the detector heights z_d.
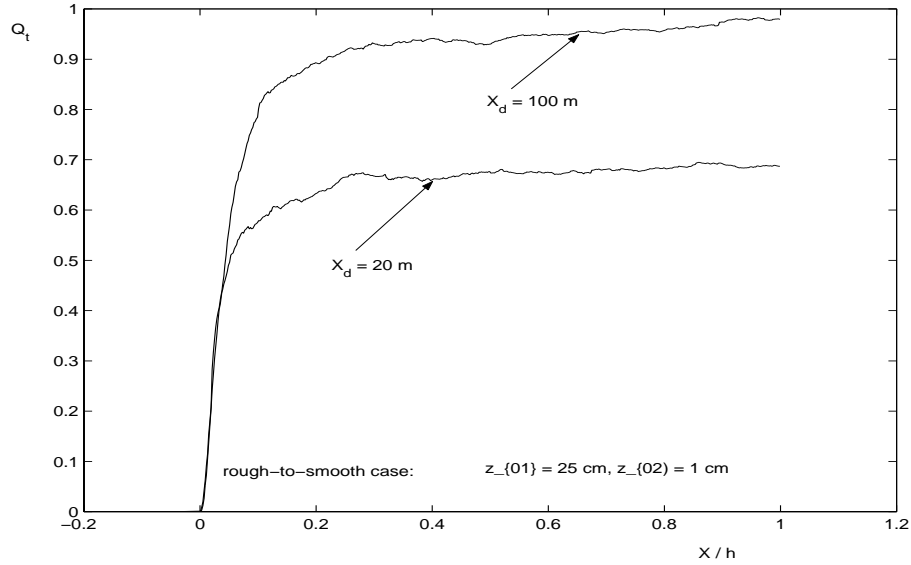

Figure 18: The cumulative footprint function of flux Q_t, the rough-to-smooth case ($z_{01} = 25$ cm, $z_{02} = 1$ cm), for $x_d = 20$ m and $x_d = 100$ m, and for the detector height $z_d = 2m$.

Appendix I. Dimensionless mean-flow equations

It is convenient to work in dimensionless variables by introducing:

$$\zeta = z/h, \ \ \xi = x/h, \ \ u_g = u/G, \ \ v_g = v/G, \ \ w_g = w/G,$$
$$b_g = b/G^2, \ \ k_g = k/Gh, \ \ l_g = l/h, \ \ m = fh/G.$$

In the dimensionaless form, the systems of equations read

$$u_g \frac{\partial u_g}{\partial \xi} + w_g \frac{\partial u_g}{\partial \zeta} = \frac{\partial}{\partial \zeta} k_g \frac{\partial u_g}{\partial \zeta} + m v_g \ ,$$

$$u_g \frac{\partial v_g}{\partial \xi} + w_g \frac{\partial v_g}{\partial \zeta} = \frac{\partial}{\partial \zeta} k_g \frac{\partial v_g}{\partial \zeta} - m(u_g - 1) \ ,$$

$$\frac{\partial u_g}{\partial \xi} + \frac{\partial w_g}{\partial \zeta} = 0 \ ,$$

and

$$u_g \frac{\partial b_g}{\partial \xi} + w_g \frac{\partial b_g}{\partial \zeta} = \alpha_b \frac{\partial}{\partial \zeta} k_g \frac{\partial b_g}{\partial \zeta} + k_g \left[\left(\frac{\partial u_g}{\partial \zeta} \right)^2 + \left(\frac{\partial v_g}{\partial \zeta} \right)^2 \right] - \frac{c b_g^2}{k_g},$$

$$l_g = \left(\frac{1}{\kappa \zeta} + \frac{h}{l_0} \right)^{-1} , \ \ k_g = C_k \, l_g \sqrt{b_g} \ .$$

with the boundary conditions:

$$u_g = 0, v_g = 0, w_g = 0, \quad \text{at } \zeta = z_0/h \ ,$$
$$u_g = 1, \, v_g = 0, \quad \text{at } \zeta = 1, \, x \le 0,$$
$$\frac{\partial u_g}{\partial \zeta} = \frac{\partial v_g}{\partial \zeta} = 0 \text{ at } \zeta = 1, \, x > 0 \ ,$$
$$\frac{\partial b_g}{\partial \zeta} = 0 \text{ at } \zeta = z_0/h \ , \text{ and } b_g = 0 \quad \text{at} \zeta = 1 \ ,$$

and $l_g = \kappa \zeta$ at $\zeta = z_0/h$.

In the stochastic Lagrangian models, the following statistical characteristics of the flow are used: the tensor $\langle u'_\alpha u'_\beta \rangle$, and the energy dissipation rate $\bar{\varepsilon}$. We extract these functions from the following closure assumptions: $\bar{\varepsilon} = cb^2/k$, and

$$\sigma_{11} = \langle (u'_1)^2 \rangle = b/C_u,$$
$$\sigma_{12} = \langle u'_1 u'_2 \rangle = -k \frac{\partial \bar{u}_{E2}}{\partial x_1}, \quad \sigma_{22} = \langle (u'_2)^2 \rangle = b/C_v,$$
$$\sigma_{13} = \langle u'_1 u'_3 \rangle = -k \left(\frac{\partial \bar{u}_{E1}}{\partial x_3} + \frac{\partial \bar{u}_{E3}}{\partial x_1} \right),$$
$$\sigma_{23} = \langle u'_2 u'_3 \rangle = -k \frac{\partial \bar{u}_{E2}}{\partial x_3},$$
$$\sigma_{33} = \langle (u'_3)^2 \rangle = b/C_w \ .$$

19

where
$$C_u = \frac{b_u^2 + b_v^2 + b_w^2}{2\,b_u^2}, \quad C_v = \frac{b_u^2 + b_v^2 + b_w^2}{2\,b_v^2}, \quad C_w = \frac{b_u^2 + b_v^2 + b_w^2}{2\,b_w^2},$$

where b_u, b_v, b_w are the universal constants in the relations $\langle u'^2 \rangle = b_u^2\,u_*^2$, $\langle v'^2 \rangle = b_v^2\,u_*^2$, $\langle w'^2 \rangle = b_w^2\,u_*^2$ which are true in the surface layer with a constavt shear $\langle u'w' \rangle = -u_*^2$. In our calculations we have taken $b_u = 2.5, b_v = 2., b_w = 1.25$ (e.g., see Kaimal&Finnigan, 1994). All the parameters $C_k, c, C_u, C_v, C_w, etc.$ were chosen to fit the theory of the surface layer with neutral stratification.

Appendix II. Lagrangian stochastic trajectory model

The main input function of the Lagrangian stochastic models is the Eulerian pdf which is in our case assumed to be Gaussian:

$$p_E(u; x) = (2\pi)^{-3/2} (det\,\sigma)^{-1/2} \exp\left\{ -\frac{1}{2}(u_i - \bar{u}_{Ei})\lambda_{ij}(u_j - \bar{u}_{Ej}) \right\} .$$

Here λ_{ij} are the elements of a matrix Λ which is the inverse to the matrix σ defined by the entries
$$\sigma_{ij} = \langle (u_{Ei} - \bar{u}_{Ei})(u_{Ej} - \bar{u}_{Ej}) \rangle ,$$
i.e., $\sigma_{ik}\lambda_{kj} = \delta_{ij}$, or in matrix form, $\sigma\Lambda = I$, I being the identity matrix. The expressions for the entries of the matrix σ are given in Appendix I.

Forward Lagrangian trajectories.

In the forward trajectory model, the governing equations are:
$$\begin{aligned} dx_i &= u_i\,dt , \\ du_i &= a_i(x, u, t)\,dt + \sqrt{C_0\bar{\varepsilon}}\,dW_i(t), \end{aligned}$$

where
$$\begin{aligned} a_i = &-\left(\frac{C_0\bar{\varepsilon}}{2}\right)\lambda_{ik}(u_k - \bar{u}_{Ek}) + \bar{u}_{Ej}\frac{\partial \bar{u}_{Ei}}{\partial x_j} + \frac{1}{2}\frac{\partial \sigma_{ij}}{\partial x_j} \\ &+ \left[\frac{\partial \bar{u}_{Ei}}{\partial x_j} + \frac{\lambda_{im}}{2}\bar{u}_{Ek}\frac{\partial \sigma_{jm}}{\partial x_k}\right](u_j - \bar{u}_{Ej}) + \frac{\lambda_{im}}{2}\frac{\partial \sigma_{km}}{\partial x_j}(u_j - \bar{u}_{Ej})(u_k - \bar{u}_{Ek}), \end{aligned}$$

Backward Lagrangian trajectories.

The backward trajectories are defined by
$$\begin{aligned} d\hat{x} &= \hat{u}\,ds. \\ d\hat{u}_i &= \hat{a}_i\,ds + \sqrt{C_0\bar{\varepsilon}}\,\overleftarrow{d}\,W_i(s), \quad s < t, \end{aligned}$$

where

$$
\begin{aligned}
\hat{a}_i &= a_i - C_0 \bar{\varepsilon} \frac{\partial}{\partial u_i} \ln p_E = a_i + C_0 \bar{\varepsilon} \lambda_{ij}(u_j - \bar{u}_{Ej}) \\
&= \left(\frac{C_0 \bar{\varepsilon}}{2} \right) \lambda_{ik}(u_k - \bar{u}_{Ek}) + \bar{u}_{Ej} \frac{\partial \bar{u}_{Ei}}{\partial x_j} + \frac{1}{2} \frac{\partial \sigma_{ij}}{\partial x_j} \\
&+ \left[\frac{\partial \bar{u}_{Ei}}{\partial x_j} + \frac{\lambda_{im}}{2} \bar{u}_{Ek} \frac{\partial \sigma_{jm}}{\partial x_k} \right] (u_j - \bar{u}_{Ej}) + \frac{\lambda_{im}}{2} \frac{\partial \sigma_{km}}{\partial x_j} (u_j - \bar{u}_{Ej})(u_k - \bar{u}_{Ek}).
\end{aligned}
$$

References

[1] Axell, L.B., and Liungman, O., 2001, "A one-equation turbulence model for geophysical applications: comparison with data and the $k - \varepsilon$ model". *Environmental Fluid Mechanics*, **1**, 71-106.

[2] Baldocchi, D., 1997, 'Flux footprints within and over forest canopies', *Boundary-Layer Meteorol.* **85**, 273-292.

[3] Flesch, T.K., 1996, 'The footprint for flux measurements, from backward Lagrangian stochastic models', *Boundary-Layer Meteorol.* **78**, 399-404.

[4] Flesch, T.K., and Wilson, J.D., 1992, 'A two-dimensional trajectory-simulation model for non-Gaussian, inhomogeneous turbulence within plant canopies', *Boundary-Layer Meteorol.* **61**, 349-374.

[5] Horst, T.W., and Weil, J.C., 1992, 'Footprint estimation for scalar flux measurements in the atmospheric surface layer', *Boundary-Layer Meteorol.* **59**, 279-296.

[6] Kaimal, J.C., and Finnigan, J.J., 1994, *Atmospheric Boundary Layer Flows. Their Structure and Measurement*, Oxford University Press, New York, 289 pp.

[7] Kaiser, J., 1998, New network aims to take the World's CO2 pulse. Science 281, 506-507.

[8] Kurbanmuradov, O., and Sabelfeld, K.K., 2000, Lagrangian stochastic models for turbulent dispersion in the atmospheric boundary layer. Boundary-Layer Meteorology, **97**, N2, 191-218.

[9] Kurbanmuradov, O., Rannik, Ü, Sabelfeld, K.K., and Vesala, T., 1999, 'Direct and adjoint Monte Carlo for the footprint problem', *Monte Carlo Methods and Appl.* **5**, N2, 85-111.

[10] Leclerc, M.Y., and Thurtell, G.W., 1990, 'Footprint prediction of scalar fluxes using a Markovian analysis', *Boundary-Layer Meteorol.* **52**, 247-258.

[11] Monin, A.S., and Yaglom, A.M., 1975, *Statistical Fluid Mechanics.* Vol. **2** M.I.T. Press, Cambridge, Massachusets.

[12] . Rannik, Ü., Markkanen, T., Raittila, J., Hari, P., and Vesala, T., 2003. Turbulence statistics inside and over forest: influence on footprint prediction. Boundary-Layer Meteorol., accepted.

[13] Rannik, M. Aubinet, Kurbanmuradov, O., Sabelfeld, K., Markkanen, T. and Vesala, T., 2000. Footprint analysis for measurements over a heterogeneous forest. Boundary-Layer Meteorology, 97, 1, 137-166.

[14] Running, S., 1998. A blueprint for improved global change monitoring of the terrestrial biosphere. Earth. Obs., 10, 8-12.

[15] Sabelfeld, K., 1991, *Monte Carlo Methods in Boundary Value problems*. Springer-Verlag, New York-Tokyo-Berlin.

[16] Schuepp, H.P., Leclerc, M.Y., MacPherson, J.I., and Desjardins, R.L., 1990, 'Footprint prediction of scalar fluxes from analytical solutions of the diffusion equation', *Boundary-Layer Meteorol.* **50**, 355-373.

[17] Schmid, H.P., 1994, 'Source areas for scalar and scalar fluxes', *Boundary-Layer Meteorol.* **67**, 293-318.

[18] Thomson, D.J., 1987, 'Criteria for the selection of stochastic models of particle trajectories in turbulent flows', *J. Fluid. Mech.* **180**, 529-556.

[19] Valentini, R., Matteucci, G., Dolman, A.J., Schulze, E.D., Rebmann, C., Moors, E.J., Granier, A., Gross, P., Jensen, N.O., Pilegaard, K., Lindroth, A., Grelle, A., Bernhofer, C., Grünwald, T., Aubinet, M., Ceulemans, R., Kowlski, A.S., Vesala, T., Rannik., Ü., Berbider, P., Lousteau, D., Guömundsson, J., Thorgeirsson, H., Ibrom, A., Morgenstern, K., Clement, R., Moncrieff, J., Montagnani, L., Minerbi, S., and Jarvis, P.G., 2000, Respiration as the main determinant of carbon balance in European forests, Nature, 404, 861-865.

[20] Wager B.G., Nadegina E.D., 1979, *Atmospheric boundary layer under horizonatal inhomogeneity.* Leningrad, Gidrometeoizdat, 1979 (Russian).